JOURNAL OF SPACECRAFT AND ROCKETS
Vol. 34, No. 6, November–December 1997

Virtual Anode in Ion Beam Emissions in Space: Numerical Simulations

Joseph Wang*
Jet Propulsion Laboratory, California Institute of Technology, Pasadena, California 91109
and
Shu T. Lai†
U.S. Air Force Phillips Laboratory, Hanscom Air Force Base, Massachusetts 01731

The plasma interactions associated with the emission of an unneutralized ion beam in space are discussed. Three-dimensional particle simulations, which follow the beam ions as well as the ambient electrons and ions in the self-consistent electric field, are performed for various emission conditions. Classical theories and laboratory experiments for one-dimensional beam flow in diodes have shown that a potential hump will form when the beam current density exceeds a critical value. When the potential hump becomes so high that the beam kinetic energy is near zero there, it becomes a virtual electrode. We show that similar characteristics are also exhibited in high-density ion beams emitted from spacecraft to space plasma, although three-dimensional effects and the ambient plasma make the interaction more complex. Once a virtual anode has formed, it will partly block the beam transmission and discharge the spacecraft potential.

Nomenclature

e = electron charge
f = fraction of J_{b0} transmitted between two electrodes
I_b, I_e = beam ion current and electron current
J_b, J_e = beam ion current density and electron current density
J_{b0} = beam ion current density at the emitter exit
J_c = current density: space-charge limit between two electrodes
$J_{e\text{inf}}$ = electron current density at the inflection point
$J_{e\infty}$, $J_{i\infty}$ = ambient electron and ambient ion current density
L = distance between two electrodes
L_{inf} = distance from electrode to inflection point
L_m = distance from electrode to potential maximum
m_e, m_i = electron and ion mass
n_b, n_e, n_∞ = number density: beam ion, electron, and ambient plasma, respectively
n_bV_b, n_eV_e = beam ion and electron flux density vectors, respectively
r_b = initial beam radius
T_e, T_i, T_b = temperature: ambient electron and ion and beam ion, respectively
v_b = beam ion particle velocity
v_{te} = ambient electron thermal velocity, $\sqrt{(T_e/m_e)}$
v_{ti} = ambient ion thermal velocity, $\sqrt{(T_i/m_i)}$
$\hat{x}_m$ = normalized potential peak distance, L_m/L or L_m/L_{inf}
λ_D = Debye length
Φ = electric potential
Φ_{b0}, Φ_{bk0} = total energy and the initial kinetic energy of the ion beam
Φ_{inf} = potential at the inflection point
Φ_m = maximum potential within the beam
Φ_s = spacecraft potential or electrode potential
ω_{pe} = electron plasma frequency, $\sqrt{(4\pi n_e e^2/m_e)}$

Received Feb. 26, 1997; revision received June 19, 1997; accepted for publication July 1, 1997.

*Senior Member of Engineering Staff, Advanced Propulsion Technology Group, MS125-224, 4800 Oak Grove Drive. E-mail: joseph.j.wang@jpl.nasa.gov. Member AIAA.
†Scientist, PL/GPSS, 29 Randolph Road. Senior Member AIAA.

Introduction

MANY space experiments and applications involve plasma beam emissions. For instance, electron and ion beam experiments have been conducted in space to study beam–plasma interactions, neutralization processes, and spacecraft charging and discharge.[1–3] This paper is concerned with the physics of unneutralized ion beam emissions from spacecraft to a low-density space plasma.

Most ion beam emitters to date are similar to ion thrusters (see Fig. 1). In an ion thruster, the ions are accelerated electrostatically by a biased grid to form a high-velocity beam, typically in the kiloelectron volt energy range. When an ion thruster is used for propulsion purposes, the beam ions are emitted along with neutralizing electrons emitted from the neutralizer. Hence, the ion beam is a quasineutral beam, and there is little space charge effect on the dynamics of the beam ions. The plasma plume emitted from an ion thruster has been the subject of many recent studies (Refs. 4–6 and references therein). However, when an ion beam emitter is used for ion beam experiments, the neutralizer is turned off. If the beam current density far exceeds that of the ambient plasma, the beam is an unneutralized beam with a net positive space charge. In this case, the beam flow characteristic is dominated by space-charge effects.

The properties of space-charge beams were first studied for high-current-density beams between two plane electrodes, i.e., diodes. It is instructive to review the classical diode theory. In a diode, a charged particle beam is emitted from an electrode toward another electrode in a vacuum tube. The physics of beam flow in a diode was presented in the classical theories of Fay et al.[7] and Salzberg and Haeff.[8] At low-current density, the potential profile along the charge flow is monotonic. When the current density increases, so does the importance of the space charge. For the special case of zero initial flow velocity, the maximum current that can be transmitted between the electrodes is limited by Child's law. In this case, the space charge prohibits further increase in current density, and the potential profile is always monotonic. If the beam has a nonzero initial velocity, the potential profile can become nonmonotonic with a potential hump appearing in between the two electrodes. At sufficiently large current density, the potential hump may become so high that the kinetic energy of the flowing charge is zero at the hump. When this happens, some charges flow backward and some forward. As a result, only part of the emitting current can be transmitted while the rest is reflected backward. Therefore, this potential hump would behave

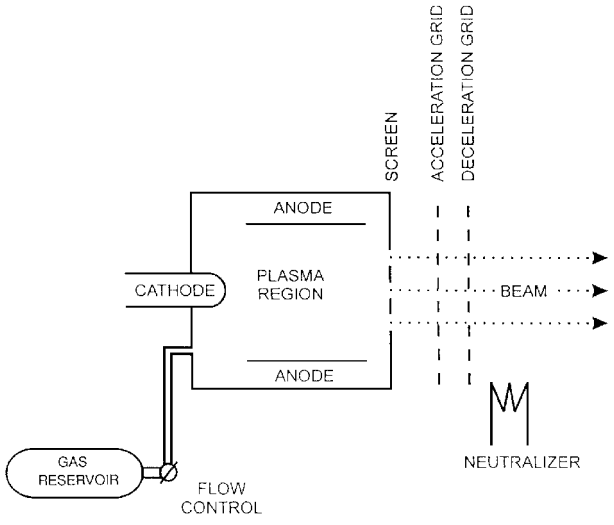

Fig. 1 Schematic of an ion beam emitter.

as a virtual electrode. The formation of virtual electrodes in diode tubes has been confirmed by laboratory experiments.[8,9]

Lai et al.[10] and Lai[11] suggested that this behavior may also occur in beam emissions in space. During ion beam experiments in space, the spacecraft is charged negatively with respect to the ambient. Hence, the spacecraft serves as a cathode and the ambient serves as an anode. Lai et al.[10] studied the current-voltage characteristics during positive ion beam emissions from the SCATHA satellite. They found that the amplitude of the negative spacecraft potential increased with the current emission at low-current levels. The potential amplitude peaked at an intermediate current. However, when the current was increased further, the potential dropped to a lower value. Because the ambient current was not sufficient to cause the discharge, it was postulated that a virtual anode may have formed in front of the beam device partly blocking the beam transmission. Stannard et al.[12] also applied the simple space charge limited diode theory to analyze the charging of the SCATHA satellite.

However, ion beam emission in space differs from the classical diode problem in two aspects. First, the beam flow in diodes is in a vacuum, and the electrodes are at fixed locations and potentials, whereas for ion beam emission in space, the ion beam flows in a low-density ambient plasma, and the location where the potential inside the beam approaches the ambient potential is a variable controlled by interactions between the beam ions and the ambient plasma. Second, the diode problem is a one-dimensional problem, whereas the problem of beam emission in space is inherently a three-dimensional one due to beam divergence caused by space-charge effects and the potential sheath profile. It is obvious that the resulting interaction is far more complex than the classical diode problem and cannot be treated adequately by the classical theory of space-charge beam flow.

In this paper we present the first three-dimensional full-particle simulations of ion beam emission from spacecraft to space plasma and examine the virtual anode concept for a three-dimensional space charge beam. The simulation model differs from those used in previous simulations of ion thruster plumes[4–6] in that we treat both electrons and ions as test particles. A one-dimensional analytical theory of space-charge beam flow is first presented, and then three-dimensional particle simulation results are discussed.

Virtual Anode in One-Dimensional Space-Charge Beams

Space-Charge Beam in a Diode

To illustrate the virtual anode concept, we first discuss the one-dimensional theory of space-charge flow of an ion beam. We first consider the situation when an ion beam is emitted in a vacuum from a plane electrode at $x = 0$ and received by a plane electrode at $x = L$. The ion beam is unneutralized and cold. The initial beam particle kinetic energy is $e\Phi_{bk0} = \frac{1}{2}mv_{b0}^2$, and the emitting current density $J_{b0} = en_{b0}v_{b0}$. We take the potential at the two ends to be $\Phi(0) = \Phi_s$ and $\Phi(L) = 0$. The steady-state solution to this problem follows the classical theory first presented by Fay et al.[7]

The governing equations are Poisson's equation, the current continuity, and the energy conservation equation,

$$\frac{d^2\Phi}{dx^2} = -\frac{en_b}{\epsilon_0} \tag{1}$$

$$n_b = J_{b0}/ev \tag{2}$$

$$e\Phi_{b0} = \tfrac{1}{2}mv_{b0}^2 + e\Phi_s = \tfrac{1}{2}mv_b^2 + e\Phi \tag{3}$$

where $e\Phi_{b0}$ is the total beam particle energy. The particle velocity is given by $v_b = \sqrt{[(2e/m)(\Phi_{b0} - \Phi)]}$. Hence, the electric potential between any two points is given by

$$\left(\frac{d\Phi}{dx}\right)^2\Bigg|_{x1}^{x2} = \frac{2J_{b0}}{\epsilon_0}\sqrt{\frac{2m}{e}}\sqrt{\Phi_{b0} - \Phi}\Big|_{\Phi 1}^{\Phi 2} \tag{4}$$

One family of the solutions to Eq. (4) is for a monotonic potential profile $\Phi(x)$. For instance, for the case $\Phi_s > 0$ and $v_{b0} = 0$, i.e., $\Phi_{b0} = \Phi_s$ and $d\Phi/dx = 0$ at $x = 0$, the solution is

$$J_{b0} = \frac{4}{9}\sqrt{\frac{2e}{m}}\frac{\epsilon_0\Phi_s^{\frac{3}{2}}}{L^2}$$

which is the well-known Child–Langmuir law of space-charge limited current in a plane diode.

A more general solution to Eq. (4) is for a nonmonotonic potential profile as illustrated in Fig. 2a. The potential takes a maximum at $x = x_m$, $\Phi(x_m) = \Phi_m > 0$. Let us define the following dimensionless variables: $\hat{x} = x/L$, $\hat{\Phi} = \Phi/\Phi_{b0}$, and $\hat{J}_{b0} = J_{b0}/J_c$, where

$$J_c = \frac{4}{9}\sqrt{\frac{2e}{m}}\frac{\epsilon_0\Phi_{b0}^{\frac{3}{2}}}{L^2} \tag{5}$$

Then, the solution is given by

$$\sqrt{\hat{J}_0}\hat{x}_m = \left(\sqrt{\Phi_{bk0}} + 2\sqrt{1 - \hat{\Phi}_m}\right)\sqrt{\sqrt{\Phi_{bk0}} - \sqrt{1 - \hat{\Phi}_m}} \tag{6}$$

$$\sqrt{\hat{J}_0}(1 - \hat{x}_m) = \left(1 + 2\sqrt{1 - \hat{\Phi}_m}\right)\sqrt{1 - \sqrt{1 - \hat{\Phi}_m}} \tag{7}$$

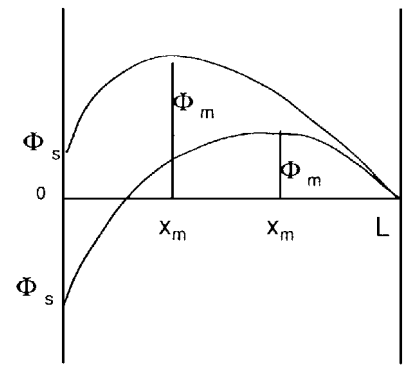

a) Beam flow between plane electrodes

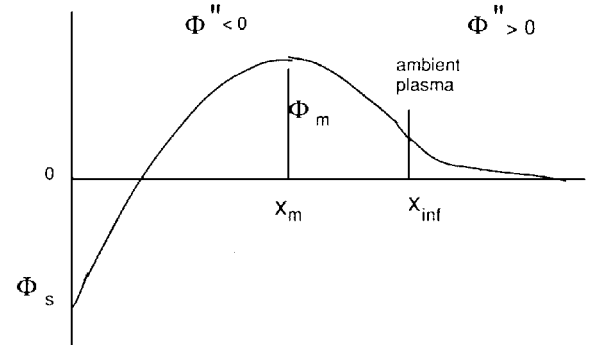

b) Beam emission into an ambient plasma

Fig. 2 Nonmonotonic potential profiles associated with a one-dimensional unneutralized ion beam.

where $\hat{\Phi}_{bk0} = mv_0^2/(2e\Phi_{b0}) = 1 - \hat{\Phi}_s$. Hence, the potential peak location is given by

$$\frac{1-\hat{x}_m}{\hat{x}_m} = \frac{\left(1+2\sqrt{1-\hat{\Phi}_m}\right)\sqrt{1-\sqrt{1-\hat{\Phi}_m}}}{\left(\sqrt{\hat{\Phi}_{bk0}}+2\sqrt{1-\hat{\Phi}_m}\right)\sqrt{\sqrt{\hat{\Phi}_{bk0}}-\sqrt{1-\hat{\Phi}_m}}} \tag{8}$$

In the limiting case $1-\hat{\Phi}_m = 0$, i.e., $\Phi_m = (m/2e)v_{b0}^2 + \Phi_s$, the ion beam comes to a halt at x_m: $v(x_m) = 0$. In this case, some ions may be reflected back at x_m, whereas others are accelerated away in the x direction. Let f be the fraction of J_0 that is transmitted through this potential barrier. Then, the beam number density is

$$n_b = \frac{J_{b0}}{ev_b} + \frac{(1-f)J_{b0}}{ev_b}, \qquad 0 < \hat{x} < \hat{x}_m$$

$$n_b = \frac{fJ_{b0}}{ev_b}, \qquad \hat{x}_m < \hat{x} < 1$$

The solution for this limiting case is

$$\sqrt{(2-f)\hat{J}_{b0}}\,\hat{x}_m = \hat{\Phi}_{bk0}^{\frac{3}{4}}, \qquad \sqrt{f\hat{J}_{b0}}(1-\hat{x}_m) = 1 \tag{9}$$

and the potential peak location is given by

$$\frac{1-\hat{x}_m}{\hat{x}_m} = \sqrt{\frac{2-f}{f}}\frac{1}{\hat{\Phi}_{bk0}^{\frac{3}{4}}} \tag{10}$$

Note that f is determined self-consistently by the space-charge current limit stated in Eq. (9). The maximum current that can be transmitted to $x = L$ is $fJ_0 = J_c$ regardless of the emitting current. Hence, J_c represents a critical current density. When the emitting current $J_{b0} > J_c$, the potential hump Φ_m serves as a virtual anode.

Space-Charge Beam in an Ambient Plasma

We next consider an ion beam emitted into a low-density ambient plasma. In this situation, the ambient plasma replaces the receiving electrode, and the electrons will move in to neutralize the excess ion space charge and, thus, modify the potential profile. However, because the electron current I_e is limited by the ambient conditions, a nonmonotonic potential profile can still exist for strong ion beam emissions, $I_b \gg I_e$. To satisfy the boundary condition imposed by the ambient plasma,

$$\Phi(\infty) = 0, \qquad \frac{d\Phi}{dx}(\infty) = 0$$

the nonmonotonic potential profile will be like that shown in Fig. 2b. We can divide the domain into a region I, $0 < x < x_{\text{inf}}$, and a region II, $x_{\text{inf}} < x < \infty$, where x_{inf} is the inflection point where the net charge is zero. There is a net ion charge surplus in region I ($d^2\Phi/dx^2 < 0$) and a net electron charge surplus in region II ($d^2\Phi/dx^2 > 0$).

Let L_{inf} denote the distance from x_{inf} to the emitting electrode ($L_{\text{inf}} = x_{\text{inf}}$ here), Φ_{inf} the potential at the inflection point, $J_{e\text{inf}}$ the electron current flowing from x_{inf} into region I, and n_e the electron density in region I. If one knew L_{inf}, Φ_{inf}, and $J_{e\text{inf}}$ a priori, the analysis for an ion beam between two plane electrodes could be applied in region I. (Such an analysis can be performed by substituting Φ with $\Phi - \Phi_{\text{inf}}$ and n_b with $n_b - n_e$ and normalizing the x with L_{inf} in all of the equations presented in the preceding section.) The condition for the virtual anode is then given by

$$J_{b0} - J_{e\text{inf}} > J_c \sim \frac{4}{9}\sqrt{\frac{2e}{m}}\frac{\epsilon_0(\Phi_{b0}-\Phi_{\text{inf}})^{\frac{3}{2}}}{L_{\text{inf}}^2} \tag{11}$$

However, x_{inf}, Φ_{inf}, n_e, and $J_{e\text{inf}}$ themselves are variables controlled by the interactions between the ion beam and the ambient plasma. Therefore, although the beam flow in region I is similar to that in the diode problem, the solution requires a self-consistent solution of both region I and region II.

For ion beam emission in space, the one-dimensional assumption is usually not acceptable because of finite beam size and beam divergence due to the space charge. The effects of beam divergence, which it is not possible to include in a self-consistent analytical formulation, are especially important in the region where the potential hump develops. Therefore, particle simulations are needed to resolve the problem of ion beam emissions in space.

Three-Dimensional Particle Simulations

We have developed a set of three-dimensional, particle-in-cell (PIC) and PIC with Monte Carlo collision codes for large-scale simulations of ion thruster plasma interactions[5,6] and active space plasma experiments.[13] To resolve the interactions between the beam ions and the ambient plasma, a full particle, three-dimensional electrostatic PIC code, which follows both the beam ions and the ambient electrons and ions, is applied in this study.

The simulation setup is shown in Fig. 3. Because our emphasis is on the near-field interactions, we set the left-side boundary of the simulation domain to be the spacecraft surface. The ion beam emitter is modeled as a three-dimensional box mounted on the spacecraft surface. The spacecraft surface and the emitter surfaces are taken to be conducting surfaces with a surface potential Φ_s relative to the ambient. All other boundaries of the simulation domain are taken to be open boundaries, which represent the ambient. A Neumann condition for electric potential is used at all open boundaries.

The simulation domain is initially loaded with test particles representing ambient electrons and ions. The ambient electrons and ions follow Maxwellian distributions. Starting from $t = 0$, the beam ion test particles are injected into the simulation domain at every time step from the emitter in the x direction. We consider a uniform beam emission and neglect beam divergence caused by the curvature of the emitter surface. The beam particles are injected to form a uniform cylindrical beam at the emitter exit with charge density $q_b n_{b0}$ and beam velocity $v_{b0}\boldsymbol{x}$. The beam ions follow a drifting Maxwellian distribution. At every time step, ambient electrons and ions are also injected into the domain from the open boundaries according to their thermal fluxes. Those test particles that hit the spacecraft or emitter surfaces or flow out of the simulation domain are deleted from the particle list.

As in a standard PIC code, the trajectories of each test particle are integrated from

$$\frac{d\boldsymbol{mV}}{dt} = \boldsymbol{F} = q\left(\boldsymbol{E} + \boldsymbol{V}\times\frac{\boldsymbol{B}}{c}\right), \qquad \frac{d\boldsymbol{x}}{dt} = \boldsymbol{V} \tag{12}$$

using a standard leapfrog scheme. The particle densities are gathered to the grid points to solve the self-consistent electric field, which is obtained from Poisson's equation

$$\nabla^2\Phi = -4\pi\rho \tag{13}$$

Then, the electric fields are scattered from grid points to particle positions for particle push at the next time step. The implementation

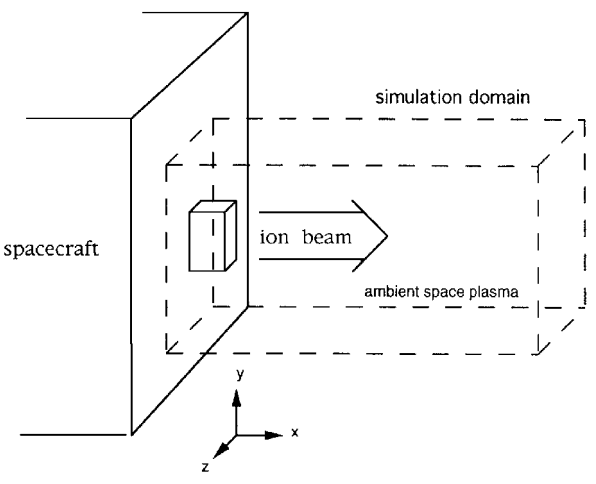

Fig. 3 Simulation setup.

of the numerical algorithm is discussed in detail in Refs. 14 and 15. The simulation is run until a steady state has been achieved.

We take the ambient plasma density $n_\infty \sim 5 \times 10^5$ cm^{-3} and ambient plasma temperature $T_e = T_i \sim 1$ eV. These parameters are similar to a typical low-Earth-orbit environment. The ambient Debye length is $\lambda_D \sim 1$ cm. The initial kinetic energy of the beam ions is taken to be $\Phi_{bk0} = \frac{1}{2} m v_{b0}^2 = 1000$ eV. The temperature of the beam ions is taken to be $T_b \sim 4$ eV. As summarized in Table 1, we shall consider three different beam current densities at beam exit, as well as three different beam sizes. We take the spacecraft potential to be $\Phi_s = -250$ V, a reasonable charging potential for a spacecraft emitting a 1-keV ion beam. Hence, the total energy of the beam at the emitter exit is $\Phi_{b0} = \Phi_{bk0} + \Phi_s = 750$ eV.

Table 1 Simulation cases

Cases	Φ_{bk0}/T_e	$J_{b0}/J_{i\infty}$	$J_{b0}/J_{e\infty}$	r_b/λ_D	Φ_s/T_e	Φ_{b0}/T_e
A1	10^3	63.25	6.33	5	−250	750
B1	10^3	316.23	31.62	5	−250	750
B2				10		
B3				2.5		
C1	10^3	3162.3	316.2	5	−250	750
C2				10		
C3				2.5		

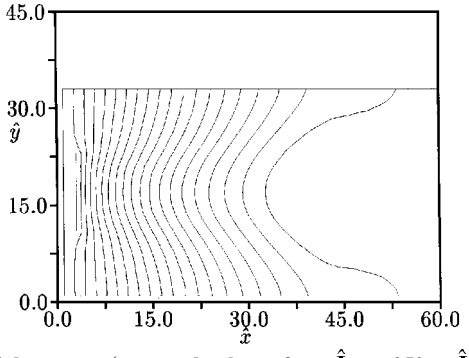

a) Potential contours (contour levels are from $\hat{\Phi} = -250$ to $\hat{\Phi} = 0$ with an interval of 12.5 and increases from left to right)

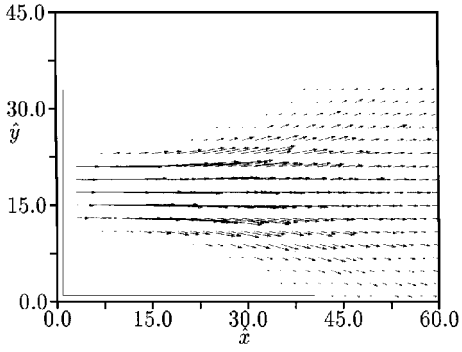

b) Beam ion current flux vectors $n_b V_b$

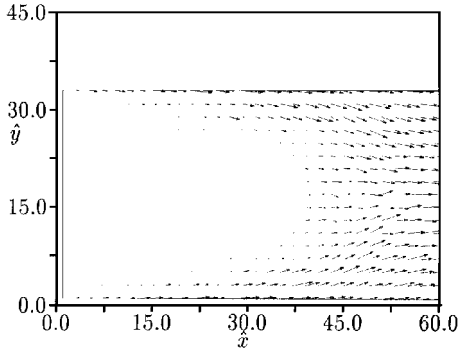

c) Ambient electron flux density vectors $n_e V_e$

Fig. 4 Simulation case A1; field plots on the center x–y plane.

The simulation variables are normalized as follows: $\hat{t} = t\omega_{pe}$, $\hat{x} = x/\lambda_D$, $\hat{v} = v/v_{te}$, $\hat{\Phi} = \Phi/T_e$, and $\hat{n} = n/n_\infty$, where $\omega_{pe} = \sqrt{(4\pi n_e e^2/m_e)}$ is the electron plasma frequency and $v_{te} = \sqrt{(T_e/m_e)}$ is the ambient electron thermal velocity. The number of grid cells used ranges from $66 \times 33 \times 33$ to $86 \times 33 \times 33$ (grid resolution $d_{\text{cell}} = \lambda_D \simeq 1$ cm). The spacecraft surface is at $\hat{x} = 0.5$. The thruster body is located at $0.5 \le \hat{x} \le 2.5$, $11 \le \hat{y} \le 23$, and $11 \le \hat{z} \le 23$. The ion beam exit surface is at $\hat{x} = 2.5$, and the beam exit center is at $\hat{x} = 2.5$, $\hat{y} = 17$, and $\hat{z} = 17$. The total number of test particles used in the simulations ranges from 1.5 to 2.5×10^6 particles. There are about 20 particles/cell representing the initial ambient plasma particles and up to 400 particles/cell representing the beam ions near the emitter exit.

As in all full-particle simulations, computational limitations require the use of an artificial ion to electron mass ratio. The artificial mass ratio compresses the relative electron and ion time scales but does not affect the steady-state solution. An artificial ion to electron mass ratio $m_i/m_e = 100$ is used ($\omega_{pe}/\omega_{pi} = 10$). Hence, the normalized initial beam velocity is $\hat{v}_{b0} = \sqrt{[(m_e/m_i)(\Phi_{ek}/T_e)]} = \sqrt{10}$. The simulation timescale is based on the electron plasma period ω_{pe}^{-1}. The time step used in the simulation is taken to be $\delta\hat{t} = \delta t \omega_{pe} \simeq 0.08$. This also ensures $v_{b0}\delta t \ll d_{\text{cell}}$. We find that a steady state is achieved after about 600–700 time steps. A series of test runs was performed with various domain sizes and resolutions, time steps, and numbers of test particles to ensure that the simulation variables do not affect the steady-state solutions.

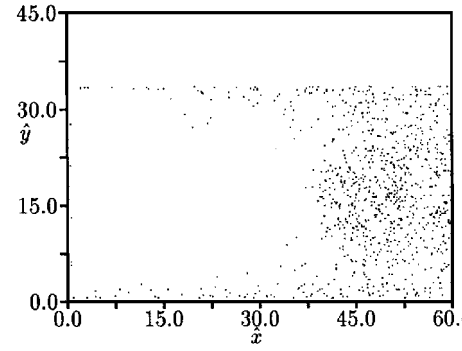

a) Ambient electron positions

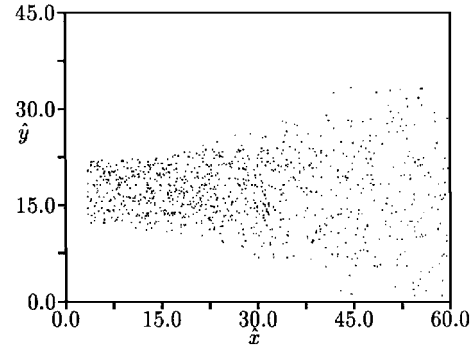

b) Beam ion positions

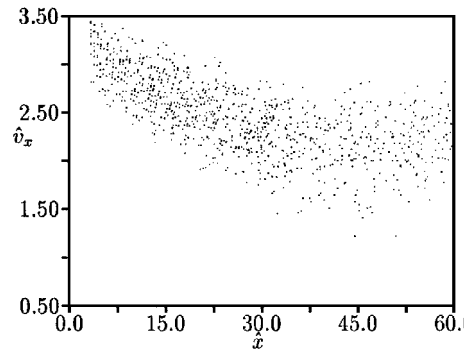

c) Beam ion $\hat{v}_{bx}$ vs $\hat{x}$ phase space

Fig. 5 Simulation case A1; particle plots on the center x–y plane.

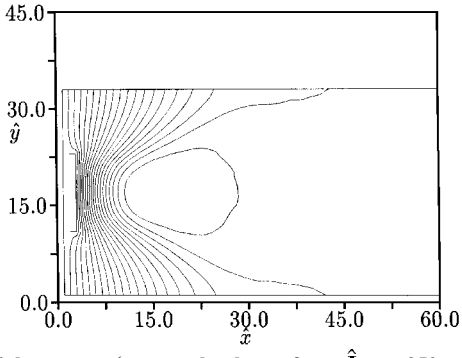

a) Potential contours (contour levels are from $\hat{\Phi} = -250$ to $\hat{\Phi} = 12.5$ with an interval of 12.5 and potential peak is at $\hat{x} \sim 15$)

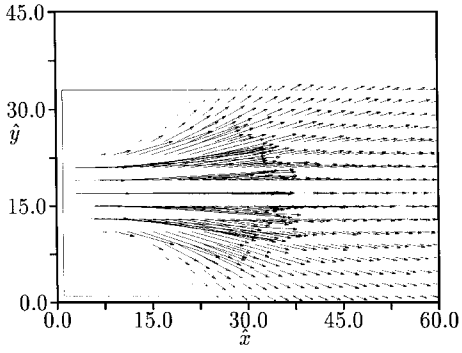

b) Beam ion current flux vectors $n_b V_b$

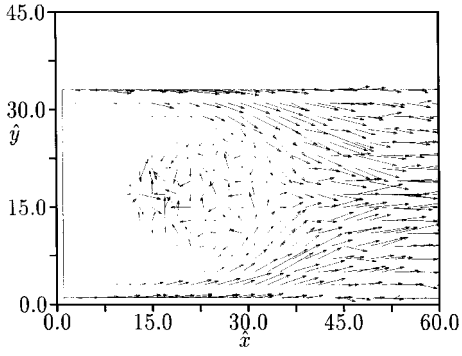

c) Ambient electron flux density vectors $n_e V_e$

Fig. 6 Simulation case B1; field plots on the center x–y plane.

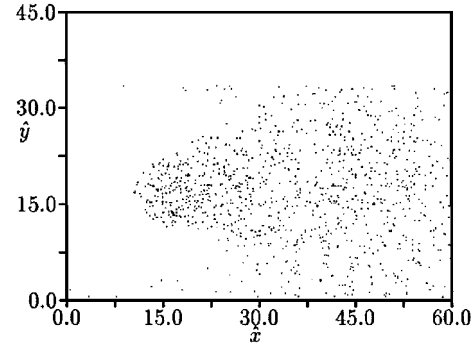

a) Ambient electron positions

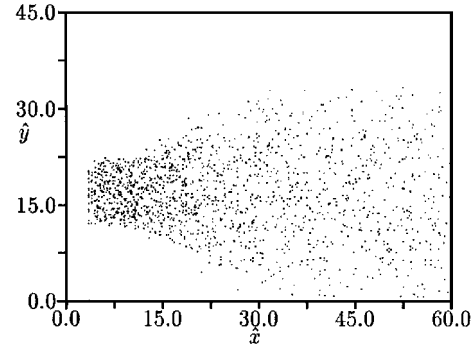

b) Beam ion positions

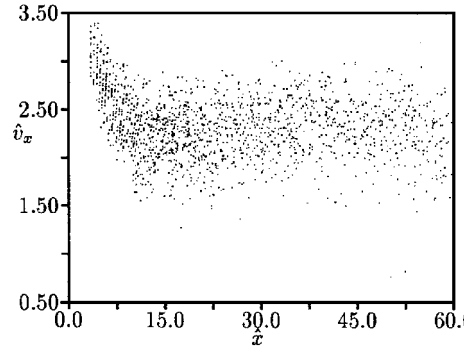

c) Beam ion $\hat{v}_{bx}$ vs $\hat{x}$ phase space

Fig. 7 Simulation case B1; particle plots on the center x–y plane.

Results and Discussion

We first consider ion beam emissions with a fixed beam radius but varying beam current densities (simulation cases A1, B1, and C1). The beam radius is taken to be $\hat{r}_b = 5$. The ratios of the beam current density, $J_{b0} = q_b n_{b0} v_{b0}$, to the ambient ion current density, $J_{i\infty} = en_\infty v_{ti}$, are $J_{b0}/J_{i\infty} \simeq 63.25, 316.23$, and 3162.3, respectively. [The ratio of J_{b0} to the ambient electron current density, $J_{e\infty} = en_\infty v_{te}$, is $J_{b0}/J_{e\infty} = \sqrt{(m_e/m_i)}\sqrt{(T_i/T_e)}(J_{b0}/J_{i\infty})$.] Because J_{b0} is much larger than the ambient electron current density, the beam is initially unneutralized.

In Figs. 4–9, we show simulation results for cases A1, B1, and C1 on an x–y plane cutting through the emitter center at $z = z_{\text{emit}} = 17$ (the center x–y plane). The results displayed include potential contours, the vector plot of the beam ion flux density $n_b V_b$ and ambient electron flux density $n_e V_e$, particle positions of the beam ions and ambient electrons, and the v_x vs x phase space plot for the beam ions. In Fig. 10, we compare the potential profiles along the downstream axis of the emitter.

In case A1 we consider a relatively low-density beam emission: $J_{b0}/J_{i\infty} \simeq 63.3$ ($J_{b0}/J_{e\infty} \simeq 6.33$). Results for case A1 are shown in Figs. 4 and 5. The potential structure in this case is dominated by the sheath due to the surface potential. However, the sheath thickness is contracted within the beam region due to high beam density. The ambient electrons are repelled toward the far right side by the negative surface potential. The ion beam space charge causes the beam to diverge near the right side of the simulation domain and draws ambient electron currents into the downstream beam region. As the $\hat{v}_x$ vs $\hat{x}$ phase space plot shows, the beam velocity decreases monotonically as beam ions escape the sheath region. The potential along the downstream axis of the emitter (Fig. 10a) shows a familiar monotonic profile for a sheath.

In case B1 we increase the beam current to $J_{b0}/J_{i\infty} \simeq 316.2$ ($J_{b0}/J_{e\infty} \simeq 31.62$). Results for case B1 are shown in Figs. 6 and 7. In this case, a positive potential hump develops near the beam exit ($\hat{\Phi}_m \simeq 24$ at a distance $L_m = \hat{x} - \hat{x}_{\text{emit}} \simeq 12.5$). A population of electrons is trapped within that potential hump. The v_x vs x phase space plot shows that the beam ions decelerate to a $\hat{v}_{\min}$ at $\hat{x} \simeq 15$. The potential along the downstream axis of the emitter (Fig. 10b) shows a nonmonotonic profile. Because $\Phi_m \ll \Phi_{b0}$, the beam still flows in the x direction. Because of the larger beam density, the space-charge effect is stronger than that in case A, which causes a larger beam divergence. The beam divergence locally shielded the effect of the spacecraft potential and results in a much thinner sheath. As a result, electrons move into a region much closer to the spacecraft.

In case C1, the ion beam emitted is $J_{b0}/J_{i\infty} \simeq 3162.3$ ($J_{b0}/J_{e\infty} \simeq 316.23$). Results for case C1 are shown in Figs. 8 and 9. In this case, a potential peak is formed at a distance of $L_m = \hat{x} - \hat{x}_{\text{emit}} \simeq 2.5$ from the beam exit. As the v_x vs x phase space plot shows, some of the beam particles are reflected back toward the emitter by the potential maximum. Hence, the potential peak has become a virtual anode in this case. As evident from the $n_b V_b$ vector plot and ion

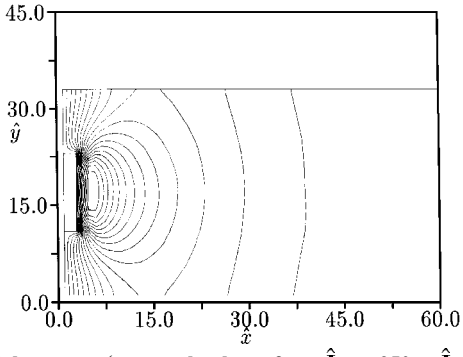

a) Potential contours (contour levels are from $\hat{\Phi} = -250$ to $\hat{\Phi} = 700$ with an interval of 47.5 and potential peak at $\hat{x} \sim 5$)

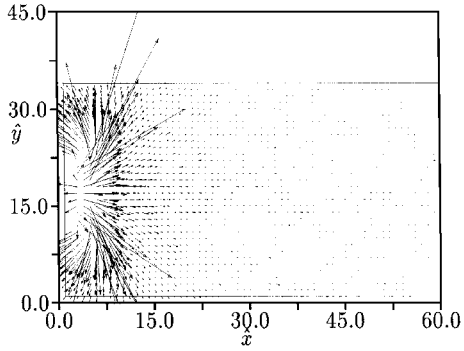

b) Beam ion current flux vectors $n_b V_b$

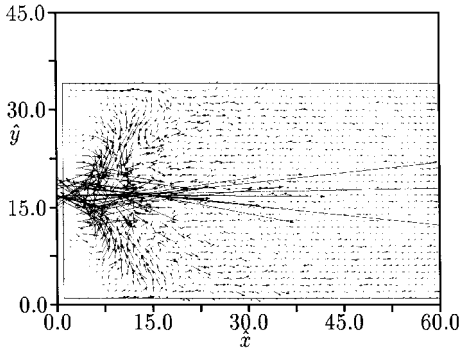

c) Ambient electron flux density vectors $n_e V_e$

Fig. 8 Simulation case C1; field plots on the center x–y plane.

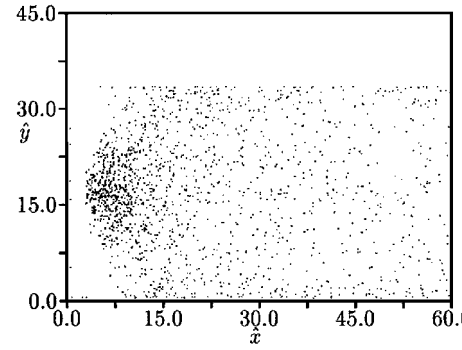

a) Ambient electron positions

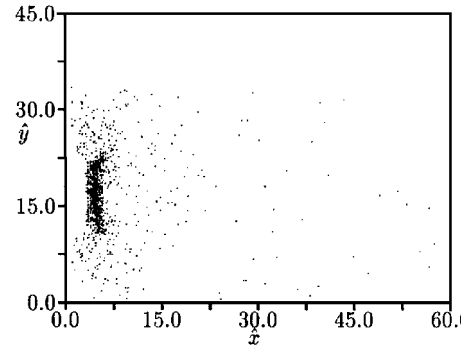

b) Beam ion positions

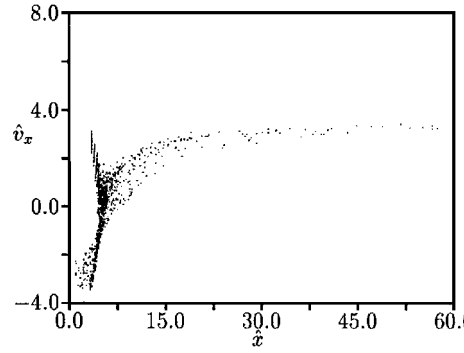

c) Beam ion $\hat{v}_{bx}$ vs $\hat{x}$ phase space

Fig. 9 Simulation case C1; particle plots on the center x–y plane.

position plot, the beam has lost its coherent structure. The ion current seems to originate from the virtual anode rather than flowing out from the thruster. On the other hand, the ambient electrons flow toward the virtual anode and fills in the vicinity of the spacecraft surface. The virtual anode reflects about 60% of the beam ions back to the spacecraft and locally shields out the ambient plasma from the spacecraft potential.

We have also run simulations for different spacecraft potentials, and the results are similar to those displayed in Figs. 4–9. Figure 10 also plots the potential profiles along the emitter downstream axis for simulations with a less negative spacecraft potential, $\hat{\Phi}_s = -50$. As evident from Fig. 10b, the effect of Φ_s is mainly on the location of the potential hump. (A more negative Φ_s moves the potential hump away from the emitter.) This is similar to the effects of the electrode potential on the one-dimensional beam flow in a diode. However, the overall interaction is still controlled by the emitting current density.

We next consider the effects of the beam radius. In cases B2 and B3, we take J_{b0} to be the same as that for case B1. However, the initial beam radius in B2 is twice that in B1, $\hat{r}_b = 10$, and the initial beam radius in B3 is half of that in B1, $\hat{r}_b = 2.5$. The results (potential contours with beam ion flux vectors) are compared in Fig. 11. (Contour levels for B2 are from $\hat{\Phi} = -250$ to $\hat{\Phi} = 300$ with an interval of 50 and $\hat{\Phi} = 320$. Potential peak is at $\hat{x} \sim 11$. Contour levels for B3 are from $\hat{\Phi} = -250$ to $\hat{\Phi} = 0$ with an interval of 25 and increases from left to right.) We find that a positive potential hump much larger than that in B1 develops in B2 ($\hat{\Phi}_m \simeq 322$ at $L_m = \hat{x} - \hat{x}_{\text{emit}} \simeq 8.5$), whereas the potential hump disappears in B3. Similarly, in cases C2 and C3, we take J_{b0} to be the same as that for C1 but $\hat{r}_b = 10$ in C2 and $\hat{r}_b = 2.5$ in C3. The results are shown in Fig. 12. (Contour levels for C2 are from $\hat{\Phi} = -250$ to $\hat{\Phi} = 700$ with an interval of 50. Potential peak is at $\hat{x} \sim 6$. Contour levels for C3 are from $\hat{\Phi} = -250$ to $\hat{\Phi} = 250$ with an interval of 25. Potential peak is at $\hat{x} \sim 7$.) As in C1, a virtual anode is formed in C2 at a distance of $L_m = x - x_{\text{emit}} \simeq 3.5$ from the beam exit. However, the virtual anode in C2 is stronger than that in C1 in that only 17% of the beam ions are transmitted to the ambient (about 70% of the beam ions are reflected directly back to the emitter surface). On the other hand, only a positive potential hump forms in C3 ($\hat{\Phi}_m \simeq 268$ at $L_m = \hat{x} - \hat{x}_{\text{emit}} \simeq 4.5$). Note that in C3 the beam radius is smaller than L_m.

The results shown in Figs. 11 and 12 are not surprising. For beams with a smaller beam radius, the effects of beam divergence are more prominent, and positive potential buildup within the beam is more easily wiped out by ambient electrons. Hence, a virtual anode or a nonmonotonic potential profile is more likely to form for beam emissions with a wider beam radius.

Although the one-dimensional space-charge theory does not apply to ion beam emissions in space, it is still interesting to compare

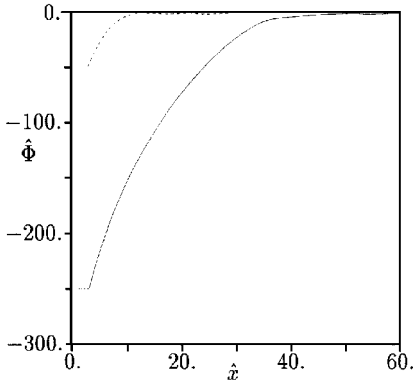

a) $J_{b0}/J_{i\infty} = 63.25$ ($J_{b0}/J_{e\infty} = 6.33$)

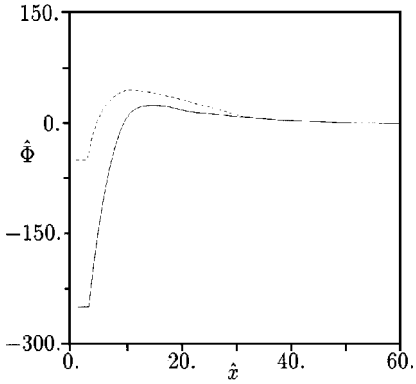

b) $J_{b0}/J_{i\infty} = 316.23$ ($J_{b0}/J_{e\infty} = 31.62$)

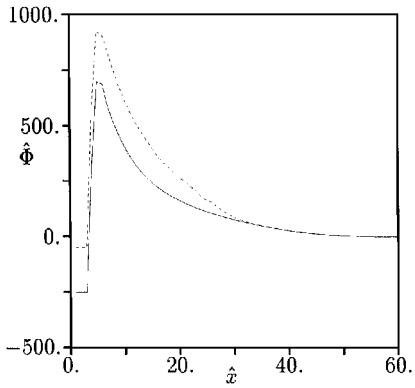

c) $J_{b0}/J_{i\infty} = 3162.3$ ($J_{b0}/J_{e\infty} = 316.2$)

Fig. 10 Potential profile along the emitter downstream axis: ——, $\hat{\Phi}_s = -250$ and ·····, $\hat{\Phi}_s = -50$.

the simulation results with the one-dimensional theory. From the simulation results, we define $L_{\inf}$ to be the distance from the beam exit to the point where the plasma first becomes quasineutral along the beam axis and $\Phi_{\inf}$ to be the potential at that point. The fraction of J_{b0} transmitted, f, is calculated from the test particles emitted and reflected by the virtual anode. To apply Eqs. (8) and (10), we use $\Phi_{\inf}$ as the potential reference and $L_{\inf}$ as the length normalization.

We take cases B2 and C2 as an example. For B2, we find $L_{\inf} \simeq 13.5$ and $\hat{\Phi}_{\inf} \simeq 297$. Applying Eq. (8), we find that $\hat{x}_m \sim 0.77$. The simulation result is $L_m/L_{\inf} \sim 0.63$. For C2, we have $L_{\inf} \simeq 11.5$ and $f \simeq 0.83$. Applying Eq. (10) we find that $\hat{x}_m \sim 0.27$. The simulation result is $L_m/L_{\inf} \sim 0.3$. Hence, the potential peak locations are in general agreement with the one-dimensional theory. Using the $L_{\inf}$ and $\Phi_{\inf}$ along the beam axis, we also estimate the one-dimensional space-charge limit current density in Eq. (11) to be $J_c/J_{i\infty} \sim 33$ for B2 and $J_c/J_{i\infty} \sim 40$ for C2, respectively. Hence, $J_{b0} \gg J_c$ in both cases. Not surprisingly, because the one-dimensional theory does not include the effects of beam divergence and the neutralizing electron current surrounding a three-dimensional ion beam, the one-dimensional space-charge limit is much lower than that for a three-dimensional ion beam in space. Hence, the one-dimensional space-charge current limit only provides a necessary but not sufficient condition for virtual anode formation. On the other hand, once a potential peak has formed, we find that the one-dimensional theory provides a good prediction of the potential peak location for those situations with $r_b > L_m$. This is because, in these situations, the beam ion flow within the distance L_m is still approximately one dimensional.

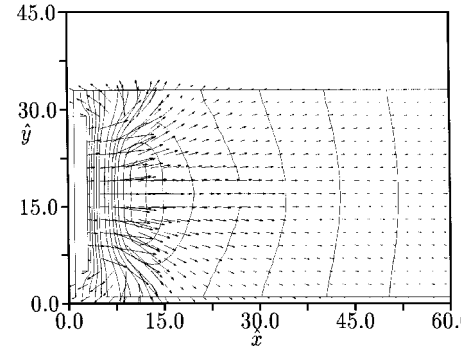

Case B2

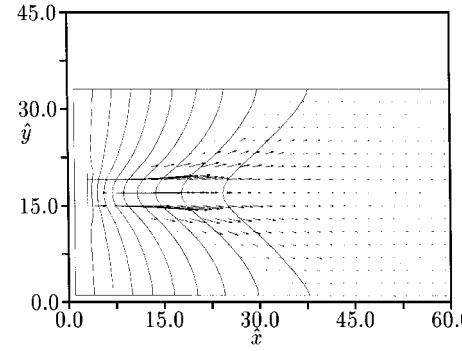

Case B3

Fig. 11 Simulation cases B2 and B3; potential contours and beam ion current flux vectors $n_b V_b$ on the center x–y plane.

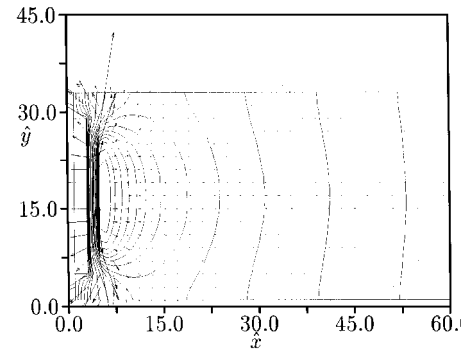

Case C2

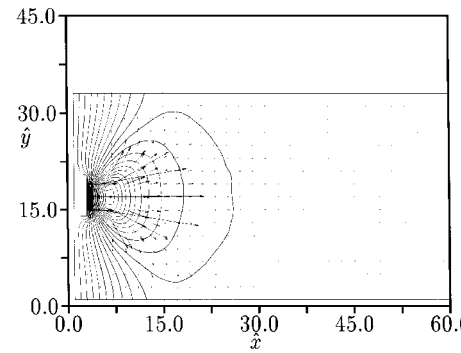

Case C3

Fig. 12 Simulation cases C2 and C3; potential contours and beam ion current flux vectors $n_b V_b$ on the center x–y plane.

Conclusions

We have developed a three-dimensional particle simulation model to study the physics of ion beam emission from spacecraft into a low-density space plasma. Unlike the situation of an ion thruster where the plasma plume is quasineutral and the beam ions simply travel along their line of sight, the ion beam emission studied here is an unneutralized beam with a net positive space charge. Our simulation follows both the beam ions and the ambient electrons and ions. A series of simulation results is presented for various emitting current densities, beam radii, and spacecraft potentials. The characteristics of the problem sensitively depend on the beam density and kinetic energy as well as the beam radius. We have demonstrated that, as the emitting current increases, the potential profile in the ion beam emitted from a negatively charged spacecraft changes from monotonic to nonmonotonic with a positive potential hump near the emitter. At a sufficiently large beam current, the potential hump can be high enough so the beam kinetic energy there is near zero. Hence, a virtual anode is formed. The spacecraft potential affects the location of the potential hump. These characteristics are similar to that of the one-dimensional space-charge beam flow in a diode. However, for ion beam emissions in space, beam divergence due to space charge and interactions between the beam and the ambient plasma make the problem much more complex. The ambient condition controls the neutralizing of the ion beam and, thus, modifies the potential profile on which the critical current for virtual anode formation depends. Comparing to the one-dimensional space-charge flow, three-dimensional effects and the self-adjustment by the ambient plasma make the conditions for virtual anode formation less favorable in ion beam emission in space. Nevertheless, the nonmonotonic potential profile is a stable potential structure. As the effects of beam divergence and electron neutralization are more prominent for beams with a smaller beam radius, a virtual anode or a nonmonotonic potential profile is more likely to form for beam emissions with a wider beam radius. Whereas the one-dimensional theory does not apply to the problem of ion beam emission in space, it may be used to predict the virtual anode location if the beam radius is sufficiently large. Once a virtual anode has formed during ion beam emission, it will partly block the beam transmission, and the beam current reflected by the virtual anode can partly discharge the negative potential of a spacecraft. Hence, the formation of a virtual anode may, indeed, be the cause of the nonmonotonic current-voltage characteristics observed during several ion beam emission experiments. This paper only considers the interactions at near field of the ion beam emitter. In the future, the analysis will be extended to study global interactions and spacecraft charging and discharge during ion beam emissions.

Acknowledgments

This work was carried out by the Jet Propulsion Laboratory, California Institute of Technology, under contract with NASA. Access to the Cray J90 supercomputer used in this study was provided by funding from NASA Offices of Mission to Planet Earth, Aeronautics, and Space Science. We wish to thank L. P. Block for helpful discussions.

References

[1] Beghin, C., Lebreton, J., Maehlum, B., Troim, J., Ingsoy, P., and Michau, J., "Phenomena Induced by Charged Particle Beams," *Science*, Vol. 225, 1984, pp. 188–194.

[2] Cohen, H. A., and Lai, S. T., "Discharging the p78-2 Satellite Using Ions and Electrons," AIAA Paper 82-0266, Jan. 1982.

[3] Katz, I., Barfield, J. N., Burch, J. L., Marshall, J. A., Gibson, W. C., Neubert, T., Roberts, W. T., Taylor, W. W. L., and Beattie, J. R., "Interactions Between the Space Experiments with Particle Accelerators Plasma Contactor and the Ionosphere," *Journal of Spacecraft and Rockets*, Vol. 31, No. 6, 1994, pp. 1079–1084.

[4] Samanta Roy, R., Hastings, D., and Gatsonis, N., "Numerical Study of Spacecraft Contamination and Interactions by Ion-Thruster Effluents," *Journal of Spacecraft and Rockets*, Vol. 33, No. 4, 1996, pp. 535–542.

[5] Wang, J., and Brophy, J., "3-D Monte-Carlo Particle-in-Cell Simulations of Ion Thruster Plasma Interactions," AIAA Paper 95-2826, July 1995.

[6] Wang, J., Brophy, J., and Brinza, D., "3-D Simulations of NSTAR Ion Thruster Plasma Environments," AIAA Paper 96-3202, July 1996.

[7] Fay, C. E., Samuel, A. L., and Shockley, W., "On the Theory of Space Charge Between Parallel Electrodes," *Bell System Technical Journal*, Vol. 17, No. 49, 1938, pp. 49–79.

[8] Salzberg, B., and Haeff, A., "Effects of Space Charge in the Grid-Anode Region of Vacuum Tubes," *RCA Review*, Vol. 2, No. 4, 1938, pp. 336–374.

[9] Intrator, T., Cho, M. H., Wang, E. Y., Hershkowitz, N., Diebold, D., and Dekock, J., "The Virtual Cathode as a Transient Double Sheath," *Journal of Applied Physics*, Vol. 64, No. 6, 1988, pp. 2927–2933.

[10] Lai, S. T., Burke, W. J., and Cohen, H. A., "A Theoretical Investigation of Virtual Electrode Formation near the SCATHA Satellite," *EOS*, Vol. 60, No. 46, 1979, p. 923.

[11] Lai, S. T., "An Overview of Electron and Ion Beam Effects in Charging and Discharging of Spacecraft," *IEEE Transactions on Nuclear Science*, Vol. 36, No. 6, 1989, pp. 2027–2032.

[12] Stannard, P. R., Katz, I., Mandel, M., Cassidy, J., Parks, D., Rotenberg, M., and Steen, P., "Analysis of the Charging of the SCATHA (p78-2) Satellite," NASA CR-165348, 1981.

[13] Wang, J., Biasca, R., and Liewer, P., "3D Electromagnetic Monte Carlo Particle-in-Cell Simulations of Critical Ionization Velocity Experiments in Space," *Journal of Geophysical Research*, Vol. 101, No. A1, 1996, pp. 371–382.

[14] Wang, J., Liewer, P. C., and Decyk, V. K., "3D Electromagnetic Plasma Particle Simulations on a MIMD Parallel Computer," *Computer Physics Communications*, Vol. 87, 1995, pp. 35–53.

[15] Wang, J., Liewer, P., and Huang, E., "3-D Particle-in-Cell with Monte Carlo Collision Simulations on Three MIMD Parallel Computers," *Journal of Supercomputing*, Vol. 10, 1997, pp. 331–348.

A. C. Tribble
Associate Editor